*Article*

# Synthesis and characterization of Cu decorated zeolite A@void@Et-PMO nanocomposites for removal of methylene blue by a heterogeneous Fenton reaction

**Xiayu Li [1], Shangjing Zeng [2], Xuejian Qu [1], Jinyu Dai [1], Xiaofang Liu [1], Runwei Wang [1,*], Zongtao Zhang [1], Shilun Qiu [1]**

[1] State Key Lab of Inorganic Synthesis and Preparative Chemistry, Jilin University, Changchun 130012, China; lixiayu24@126.com (X. L); inorg@jlu.edu.cn (X. Q.); 1519486944@qq.com (J. D.); 1337267539@qq.com (X. L.); zzhang@jlu.edu.cn (Z. Z.); sqiu@jlu.edu.cn (S. Q.)

[2] Key Laboratory of High-Performance Synthetic Rubber and its Composite Materials, Changchun Institute of Applied Chemistry, Chinese Academy of Sciences, Changchun 130012, Jilin,China; sjzeng@ciac.ac.cn (S. Z.)

**\*** Correspondence: rwwang@jlu. edu. cn (R. W.); Tel.: +86-431-8516-8115

**Abstract:** The development of novel porous composite materials for organic dye degradation and removal has received increasing attention due to water contamination problem. In this paper, hydrothermal synthesized nano zeolite A have been encapsulated with porous periodic mesoporous organosilica (PMO) through a simple modified StÖber method an organosilane-directed growth-induced etching strategy, the obtained yolk-shell structured sample was further functionalized by the impregnation of copper, realizing the composite material with hierarchical porous and catalytic properties. The morphology, porosity and metal content of the zeolite Cu/A and Cu/A@Et-PMO were fully characterized. As compared to the parent material, the composite Cu/A@Et-PMO have an efficient adsorption and catalytic degradation performance on methylene blue (MB), the removal efficiency reached as high as 95% of 60 mg/L MB with 10min. These novel structured porous composites may have great potential for adsorption and degradation application including waste effluents.

**Keywords:** Fenton reaction; yolk-shell structure; zeolite A; PMO

## 1. Introduction

As known, hundreds of synthetic compounds generate a series of problems and hazards for environment and ecosytem with rapid develpoment of industrials, such as toxic organic dyes, heavy metal ions, acidity or alkali compounds and the other high refractory organic compounds. It is reported over 1000 types of dyes and pigment were used worldwide and even over the $7\times10^5$ tons of colored dyes were produced annually in different industries including manufacturing, printing, and textile and so on [1]. In addition, the high toxicity of organic compounds have a serious threat to the aquatic life and human health. Therefore, it is necessary to arouse great attention to remove

contaminants in water. In fact, the organic dye compounds such as MB, methyl orange (MO) and Rhodamine B (RhB) were especially stable and refractory because their specially aromatic structure and hard to be degraded using biological, physical method [2-7]. Hence, it is imperative to develop a suitable and efficient method to treat these dyes from effluents.

Now, the combination of adsorption and degradation methods have been widely used in the treatment of effluents, owing to their efficient performances [8]. The degradation reaction occurs via generating massive free hydroxyl radical ($\cdot$OH) from hydrogen peroxide with the presence of metal catalysts, which is the essential parts of the Fenton reaction [9-11]. For degradation reaction, the synergy of the adsorption process is attributed to increasing the degradation efficiency [12]. In other words, it is desirable to obtain multi-functional catalysts through architecturing with enhanced activities both on adsorption and catalysis.

Zeolite A, as a common microporous adsorbent, is used to treat effluents including different organic pollutant dyes and pigments [13-15]. But the relatively small channels of zeolites could restrict the circulation of substrate when the slightly bulk molecules reactant exist and limited pore volume further have a negative impact on the adsorption and catalytic performance [16-18]. Therefore, nano-sturctured hierarchical porous composites have been gained much attentions due to preferable removal efficiency, expecially dealing with high concentration of organic dyes [19-24].

Herein, we first report on the synthesis of yolk-shell structured zeolite A@Et-PMO composite with nano zeolite A as the core and mesoporous organosilica as the shell via a organosilane-directed growth-induced etching strategy. The void of zeolite core and mesoporous shells gives rise to a high pore volume. Their catalytic performance for degradation of MB were evaluated after they were introduced with Cu nanoparticles. Secondary porosity, hydropobicity and active sites in shell allows this novel composite material remove MB with high efficiency. This method might be potentially useful for designing efficient multi-functional catalysts for more catalysis.

## 2. Experimental Procedure

### 2.1 Materials

Cetyltrimethyl-ammonium bromide (CTAB, 99%), tetraethylorthosilicate (TEOS, 98%) and methylene blue (MB, 99%) were purchased from Sinopharm Chemical Reagent Co. Ltd. Sodium hydroxide (NaOH, 99%), ammonium hydroxide (NH$_3$·H$_2$O, 25%), and ethanol (EtOH, 99%) were obtained from Beijing Chemical works, Beijing, China. 1,2-Bis(triethoxysilyl)-ethane (BTEE, 97%) was purchased from Adamas Reagent, Co. Ltd. Tetramethylammonium hydroxide pentahydrate (TMAOH, 25wt% aqueous soluton) was the struture directing agent (Kente Catalytic Material Co. Ltd). Silica gel (Shanghai Macklin Biochemical Co. Ltd) and aluminium isopropoxide (Tianjin Guangfu Regent Co. Ltd) was used as silica and aluminum sources, respectively. Copper(II) nitrate trihydrate and hydrogen peroxide (H$_2$O$_2$, 30%) were purchased from Xilong Scientific Co. Ltd.

### 2.2 Synthesis of zeolite A

0.2g of NaOH was dissolved in 18ml of deionized water. Then 54.2g of TMAOH was added into the aqueous solution and stirred at room temperature for 30min. The solution was subsequently divided into two equal parts. The Silica gel and aluminium isopropoxide were added into the two solution, labeled A, B, respectively. Then the solution A was added into solution B under stirring at

room temperature and the uniform solution was placed into a Teflon container after 2h.The stainless steel autoclave was placed 24h at room temperature, then transferred in constant temperature oven at 100°C for 24h. Finally, the white powder was collected by centrifugation, washing with water and ethanol for 4 times and dried at 80 °C and calcined at 550°C in air for 6h.

*2.3 Synthesis of Yolk-Shell A@Et-PMO nanocomposites*

The mesoporous $SiO_2$ layers was coated on the surface of LTA zeolite nanoparticle cores which were synthesized by a hydrothermal method via the StÖber method in supplementary text 1. Then the above sample 100 mg was dispersed in the same system of deionized water and ethanol (2:1) by ultrasonication for 30 min. The solution was stirred for 30 min after the addition of 0.12 g of CTAB and 2 mL of ammonium aqueous solution (25%-28%). Then 0.08 mL of BTEE was added dropwise into the former mixture, stirred at room temperature for 2 h. Next, the uniform solution was placed into a stainless steel autoclave with a Teflon container and hydrothermally treated at 100°C for 24 h following the above.

*2.4 Synthesis of catalytic nanoreactor Cu/A@Et-PMO composites*

The catalytic nanoreactor was prepared by traditional impregnation and reaction. 100 mg of as-prepared materials (A@Et-PMO, zeolite A) was homogeneously dispersed in the 20 mL of ethanol by ultrasonication for 30 min. After addition of a certain amount of aqueous solution copper (II) nitrate trihydrate (33.75 mmol/L), the mixture was stirred for 2 h and then green powder was get by rotary evaporation. The resulting catalysts were designated as Cu/A@Et-PMO, Cu/A, respectively.

*2.5 Degradation experiment*

The catalytic activity of the Cu/A and A@Cu@Et-PMO was demonstrated by heterogeneous Fenton degradation experiment. The reaction was carried out in 100 mL glass flask, containing 30 mL of certain concentration aqueous MB, 30 mg of nanocomposites.Then the stirring device was starting at room temperature when 3 mL of $H_2O_2$ (30 wt.%) was added into the mixture, that is time was zero. For a given time interval for 10min, a small quantity of the mixture solution was pipetted into a quartz cell (path length 1.0 cm and dull polish on both sides). The degradation percentages (D%) and MB concentration were measured through absorption spectrum by UV-vis spectrophotometer at 664 nm, which was calculated according to the equation as follows:
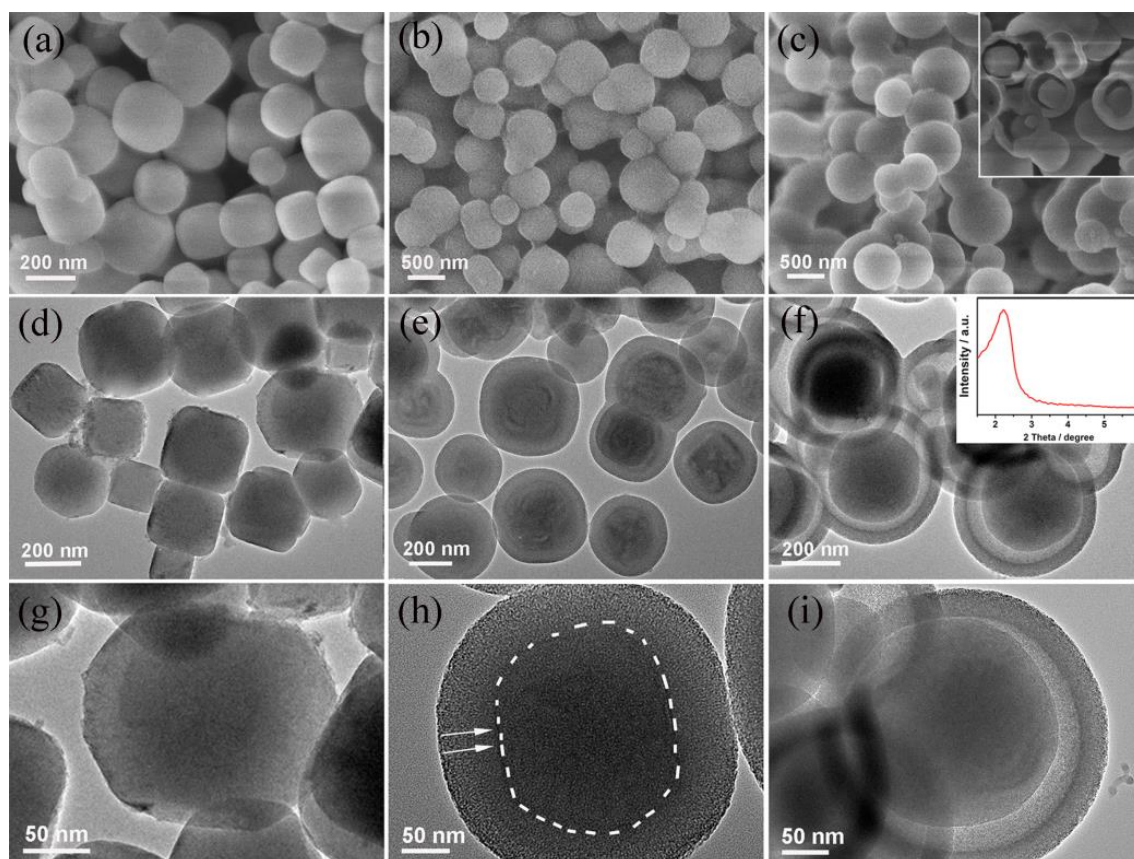
$$D(\%) = \frac{C_0 - C_t}{C_t} \times 100\% \tag{1}$$

Where $C_0$ (mg/L) and $C_t$ (mg/L) are the initial and the instantaneous concentrations of MB, respectively.

3. **Results and Discussion**

*3.1 characterization of structure A@Et-PMO*

Obviously, the zeolite A nanocrystalline particles with typical approximate squareas well as regular shape with size of 230-490 nm were observed in Figure 1a, 1d, 1g. Subsequently, We can observe the smooth surface nanospheres different to pristine zeolite A square shape with the $SiO_2$

layer about 50 nm, as shown in Figure 1b, e, indicating the core-shell structure A@mSiO$_2$ was formed.
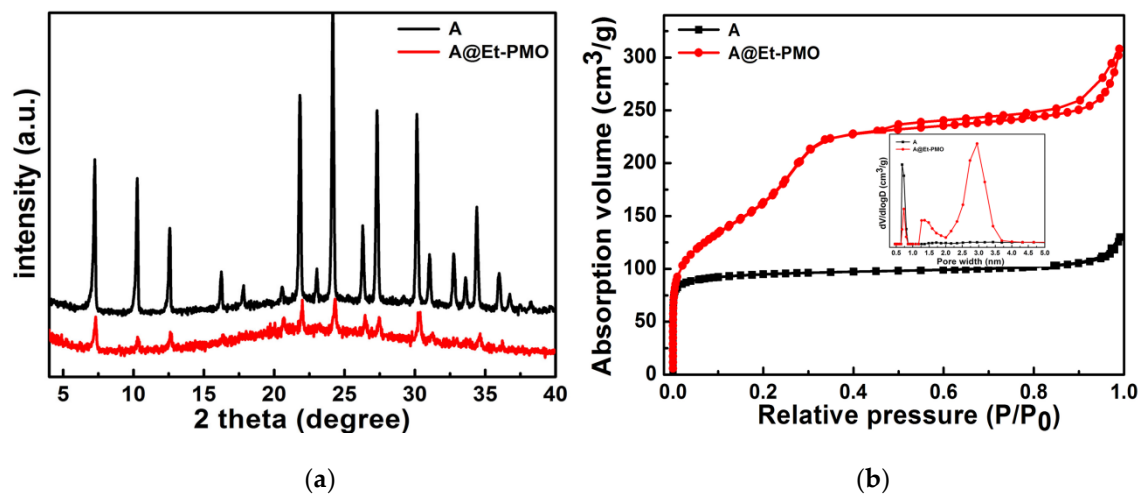


**Figure 1.** SEM images of pristine zeolite A (**a**); A@mSiO$_2$ (**b**); A@Et-PMO and the inset of the fragment of A@Et-PMO (**c**); low moderate and high magnification TEM images of prinstine zeolite A (**d**, **g**); A@mSiO$_2$ (**e**, **h**); A@Et-PMO (**f**, **i**); and the small-angle XRD pattern (inset) of A@Et-PMO (**f**).

Finally, the yolk-shell A@EtPMO was successfully generated with a diameter of 400-550 nm under basic condition. In fact, the mesosilica shell of A@mSiO$_2$ was dissolved gradually and part of dissolved silica species was inserted into generated PMO shell by co-condensation with hydrolyzed organosilane oligomers at the same time [26]. The hollow void space is almost equal to the thickness of the SiO$_2$ layer. Some broken particles from the inset image (Figure 1c and 1f) displayed visually a yolk-shell structure with core zeolite A, hollow space and outer shell. From the TEM images of A@mSiO$_2$ and A@Et-PMO, as shown in Figure 1h and 1i, we can deserve the mesochannels are perpendicular to the surface of zeolite A. The small-angle XRD pattern exhibits one sharp diffraction peak with high intensity and one weak diffraction peak at 2θ values of 2.2 and 4.4 degrees, respectively in Figure 1f inset, indicating a ordered mesopore array in A@Et-PMO shell, which is in consistent with TEM results. These results indicate that we have successfully obtained yolk-shell A@Et-PMO with core of zeolite A and uniform thickness (~40 nm) shell of Et-PMO, as well as the spacious void space owing to etched of mesopore silica layer.

The unique structure of A@Et-PMO was further confirmed by small/wide-angle X-ray diffraction and nitrogen sorption analysis. From the wide XRD pattern for A@Et-PMO (Figure 2a), some characteristic diffraction peaks contributing to zeolite A are reserved [27]. The result

demonstrates that the crystal of zeolite A is well retained throughout all synthesis process. However, the lower diffraction intensity is probably due to the shielding effects of the shell [25].



**Figure 2.** (**a**) Wide-angle XRD patterns of zeolite A and A@Et-PMO; (**b**) Nitrogen adsorption-desorption isotherms and the corresponding pore size distributions (inset) for A@Et-PMO.

The nitrogen adsorption-desorption isotherms (Figure 2b) for yolk-shell A@Et-PMO shows type I curve with a sharp up shake in the $P/P_0$ range 0-0.01, corresponding initial zeolite A, indicating the typical microporous material. Moreover, there is an addition of type IV isotherm curves with a typical capillary condensation at moderate $P/P_0$ range of 0.2-0.8, which is the unique characteristic of mesoporous material. The distinct H3 hysteresis loop indicates that the pores in Et-PMO shell open into the interior, facilitating that a guest molecular quickly diffuses between reactants without any obstacle. In contrast with pristine zeolite, the pore size distribution calculated corresponding to DFT shows two diameter types which one is caused from micropore in zeolite (about 0.68 nm) and another is attributed to the mesoporous shell approximately 2.6 nm, respectively. The A@Et-PMO exhibit higher BET surface area (686.61 $m^2/g$) and total pore volume (0.47 $cm^3/g$) compared to initial micropore material (Table 1) which provide the favorable condition for the excellent absorption performance [19]. In summary, these characters indicate that the microporous and mesoporous bimodal pore nanocomposites have been successfully prepared, that is in coincidence with the SEM and TEM results at above.

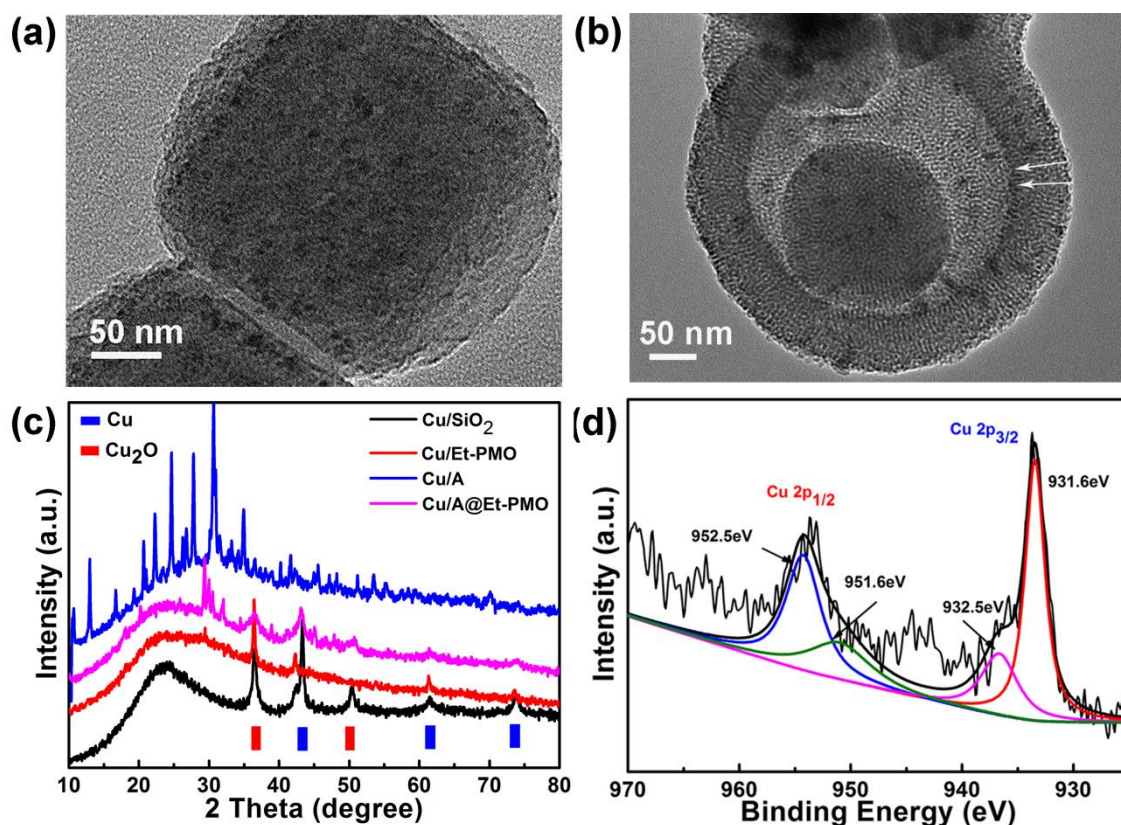**Table 1.** Textural properties of pristine zeolite A and yolk-shell structured A@Et-PMO

| Sample | $S_{BET}$ ($m^2/g$) | Smicro ($m^2/g$) | Sext ($m^2/g$) | $V_{tatol}$ ($cm^3/g$) | $V_{micro}$ ($cm^3/g$) |
|---|---|---|---|---|---|
| A@Et-PMO | 686.61 | 178.19 | 424.68 | 0.469 | 0.037 |
| Zeolite A | 300.96 | 250.41 | 50.55 | 0.174 | 0.136 |

The chemical environment of the A@Et-PMO nanocomposite was characterized by Fourier-transform infrared (FT-IR) (Figure S1). There are two weak peaks at 400-700$cm^{-1}$ related to the symmetric stretch vibrational modes of Si-O-Si and Si-O-Al groups [28], indicating the remain of zeolite A. Furthermore, additional several peaks, of which the spectra region in 2925-2850$cm^{-1}$ and at 1410$cm^{-1}$ and at 1160$cm^{-1}$, are attributed to the C-H vibrations, -$CH_2CH_2$-, respectively. The characteristic peaks at 1160-1060 $cm^{-1}$ and

695-790cm$^{-1}$ can be assigned to the vibration of Si-C and Si-O, respectively. These results demonstrate that the ethylene organic groups have been successfully incoporated into the Et-PMO shell hybrid framework, which could demonstrate the amphiphilic shell of composites caused by the hybrid of inorganic and organic framework [29]. The amphiphilic shell could strengthen the interaction between dyes and absorbents and promote the absorption of organic dyes.

### 3.2 Characterization of adsorption-degradation agent Cu/A@Et-PMO

In view of good adsorption property, the nanocomposites with zeolite A cores and Et-PMO shells can be served as a support for copper ions converted into metal nanoparticles by impregnation and reaction, which are essential element for Fenton-like reaction system to degrade organic wastes. It can be clearly observed that the copper and cuprous oxide nanoparticles with a range size of 2-4 nm are anchored into A@Et-PMO, some are loaded on the mesochannels, others may locate on the zeolite A and a little diffuse into the hollow cavity (Figure 3b). The metal nanoparticles with size of 5nm also disperse on the the zeolite, as shown in Figure 4a. The metal seed is grew in the the mesopores and the diameter of particles are relatively small, which is beneficial to enhanced degradation performance of nanocomposites [26].



**Figure 3.** (**a**) The TEM image of Cu/A; (**b**) Cu/A@Et-PMO; (**c**) wide-angle XRD patterns of four diffrent as-product; (**d**) XPS spectra of Cu/A@Et-PMO.

In order to obtain an insight into the valent state of metal copper in the catalyst Cu/A@Et-PMO, the wide XRD patterns was performed (Figure 3c). The typical diffraction peaks at 2θ values of 43.3, 50.5 and 74.1 degrees are attributed to the nanocrystalline nature of cubic phase of Cu (JCPDS No.

04-0836) corresponding to (111), (200) and (220) planes. Furthermore, the sharp peaks were observed which is in accordance with the (110) and (220) diffraction of cubic $Cu_2O$ phase [30]. Obviously, the copper ions maybe decorate on the supporting materials in form of bare $Cu^0$ and $Cu_2O$. In addition, the broad peaks at approximately 22.8 degrees, referring to the amorphous structure, is the characteristic of typical materials from sol-gel processing [31]. The diffraction peaks of Cu/A@Et-PMO and Cu/Et-PMO are lower than that of $Cu/SiO_2$, which due to the nanoparticles are highly dispersed into pore channels and the diameter of samples is smaller. And the related nitrogen sorption analysis datas of Cu/A@Et-PMO was listed in Table S1. The surface area and pore volume of materials after loading metal nanoparticles silghtly reduce due to the occupation of surface.
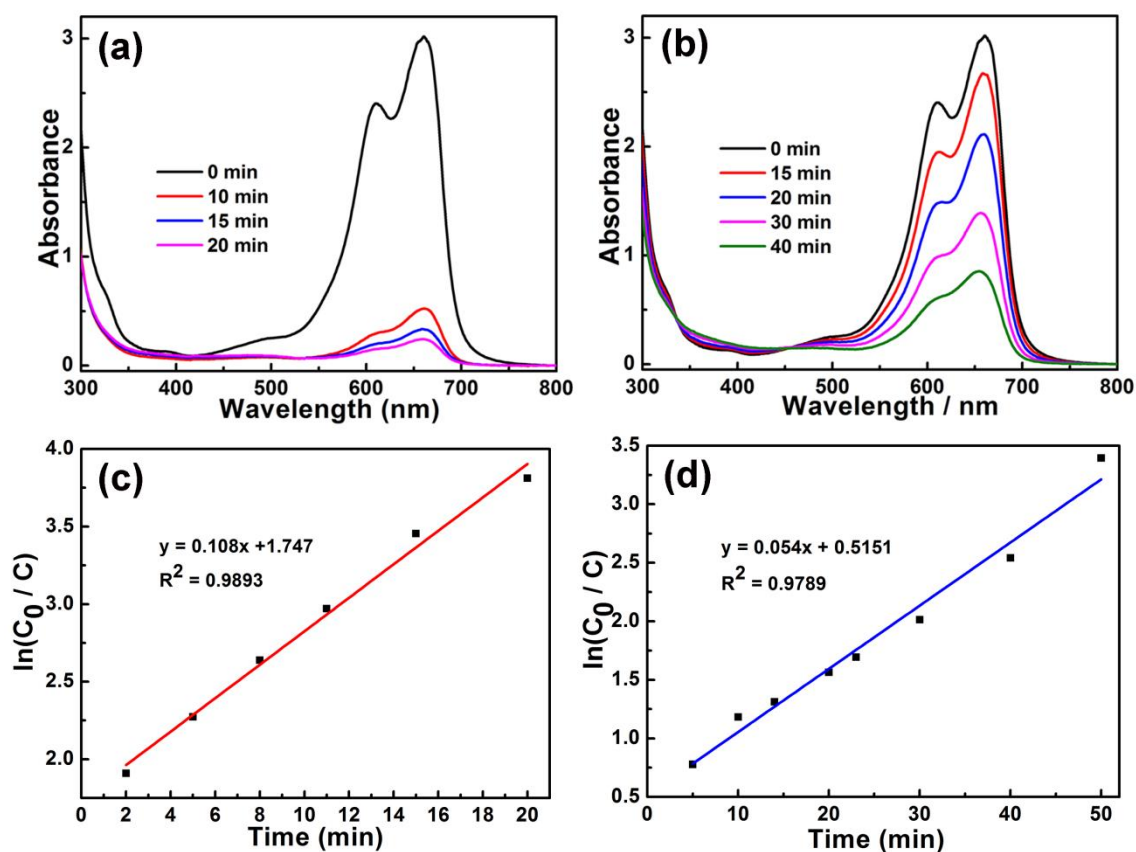
In addition, we further confirmed the oxidation states of copper by combining the XPS results, as shown in Figure 3d. The characteristic peaks of XPS spectrum for Cu 2p is asymmetrical, indicating that the form of copper is more than one and the copper ions were partly reduced to zero valent copper. The broad peaks can be seprated into two type peaks corresponding monovalent copper and zero valent copper. The binding energy of 932.5 eV and 952.5 eV is attributed to Cu $2p_{3/2}$ and Cu $2p_{1/2}$, which is corresponding to the characteristic peaks of zero valent copper [32]. In addition, the another two peaks at 931.6 eV and 951.6 eV are assigned to Cu $2p_{3/2}$ and Cu $2p_{1/2}$ corresponding to the $Cu^+$ [33]. It makes a clear that the final immobilized Cu through precipition and reduction is anchored into the nanocomposites in form of hybrid phase $Cu^0$ and $Cu^+$, which is accordance with the wide XRD result datas (Figure 3c). Moreover, the content of copper for samples are nearly same among each other identified by ICP and listed in Table S2.

### 3.3 Catalytic performance of degradation for MB

To investigate the Fenton-like catalytic performance of Cu/A@Et-PMO for the degradation of organic dye MB with the help of $H_2O_2$, we have carried out certain experiment, as shown in Figure 4a and 4b. Dramatically, the removal efficiency was calculated to be 95% at 10 min over the Cu/A@Et-PMO, while about 81% removal efficiency over Cu/A was obtained after 40 min. In addition, the kinetics of MB degradation for Cu/A@Et-PMO and A/Cu followed the pseudo-first-order kinetic equation as given by equation (2) [34]:

$$\ln(C_0/C_t) = kt \tag{2}$$

In this equation, $C_0$ (mg/L) and $C_t$ (mg/L) are the concentration of MB at the initial time (t=0) and certain time (t), and k is the kinetic rate constant, respectively. The rate constants (k) and correlation coefficients are listed in the Table 2. Obviously, the rate constant of Cu/A@Et-PMO is approximately double than that of A/Cu, 0.108 $min^{-1}$ and 0.054 $min^{-1}$ (Figure 4c and 4d), respectively, demonstrating the degradation rate for MB of Cu/A@Et-PMO is considerably higher than that of A/Cu. Apparently, the adsorption and degradation property for Cu/A@Et-PMO is superior to the pure Cu/A for MB, which can be related to the high specific surface area and large pore volume, related to strong synergistic effect in the PMO shell. Moreover, the presence of massive hydroxyl groups interact with the cationic MB dye through hydrogen bonding and electrostatic interactions, facilitating the adsorption of MB [35].

**Figure 4.** Time-dependent UV-vis spectra for the degradation of 60 mg/L of MB by 30 mg of (**a**) Cu/A@Et-PMO and (**b**) Cu/A; (**c**) and (**d**) the respective plots of In ($C_0$/C) vs. reaction time.

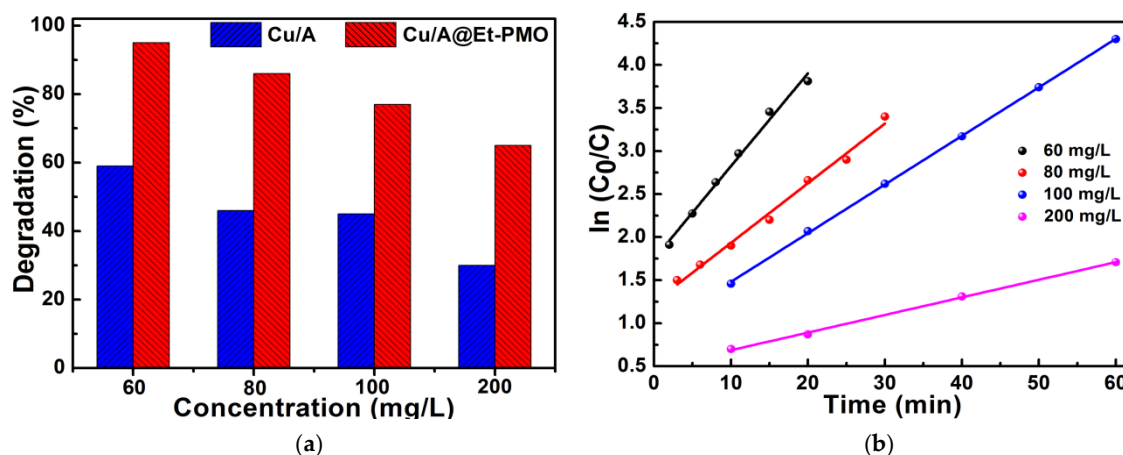**Table 2.** Completion time and rare constants of Cu/A@Et-PMO and A/Cu.

| Sample | Correlation coefficient[a] | Rate constant (k) (min$^{-1}$) |
|---|---|---|
| Cu/A@Et-PMO | 0.9893 | 0.108 |
| A/Cu | 0.9789 | 0.054 |

[a]

Correlation coefficients of the Peseudo first kinetic plots shown in figure 4c and 4d. Reaction condition: 30 mL of 60 mg/L MB, 3 mL of $H_2O_2$, 30mg catalysts at room temperature 25℃.

Comparison with Cu/A, the Cu/A@Et-PMO can remove high concentration of MB with a short time, as shown in Figure 5a. It can be observed that the final removal efficiency were 95.2%, 86.3%, 76.8%, 64.9% for Cu/A@Et-PMO, while the values were 58.9%, 46.1%, 48.7%, 30.4% over Cu/A as the initial MB concentration increased from 60 mg/L to 200 mg/L. That results could be due to the limited availability of hydroxyl radicals [36]. It also may be ascribed to competitive adsorption among dye molecules on the limited reaction area of catalyst when dealing with high concentration dye [37]. Notably, the datas indicate that Cu/A@Et-PMO has an advantage over Cu/A while conducted in high concentration dye, futhermore revealing the enhanced catalytic performance of Cu/A@Et-PMO owing to its typical yolk-shell structure in the Fenton-like reaction system. And the removal rate constants (Figure 5b) for 60 mg/L, 80 mg/L, 100 mg/L and 200 mg/L of MB by

Cu/A@Et-PMO is 0.108 min$^{-1}$, 0.069 min$^{-1}$, 0.057 min$^{-1}$ and 0.023 min$^{-1}$, respectively, indicating that the removal rate gets low with the increase of the concentration of MB.
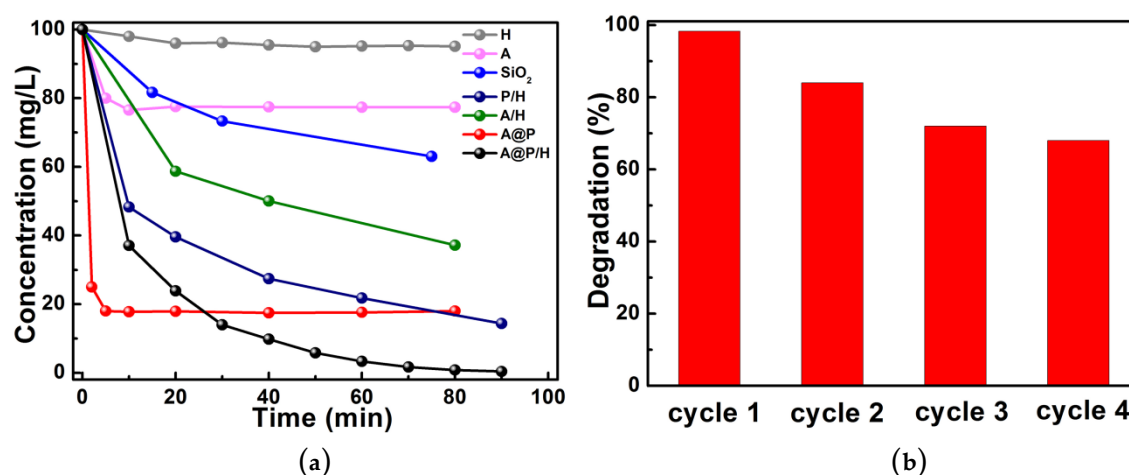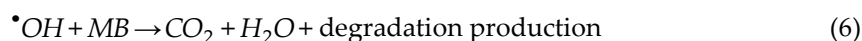


**Figure 5**. For 60 mg/L, 80 mg/L, 100 mg/L and 200 mg/L of MB (**a**) the degradation efficiency over 10 mg of A@Cu@Et-PMO and 10 mg of A/Cu within10 min; (**b**) the respective plots of In ($C_0$/C) vs. reaction time by Cu/A@Et-PMO (30mg).

*3.4 A comparative study*

To further investigate the effect of different compounds during degradation reaction, different materials including Cu/SiO$_2$, Cu/A, Cu/Et-PMO and Cu/A@Et-PMO were applied for removal of MB, respectively, as shown in Figure 6a. There was a little degradation of MB with the presence of H$_2$O$_2$ alone due to the lower generate rare of ·OH. With the absence of H$_2$O$_2$, the zeolite A showed the lower removal efficiency since it only can remove MB by adsorption, while the A@Et-PMO can remove about 80% of MB, which mainly depended on its unique characteristic of large specific area as well as the amphiphilic shell. Then, with the presence of H$_2$O$_2$, the Cu/SiO$_2$/H$_2$O$_2$ displayed lower removal efficiency, it can be explained that the size of copper nanoparticles have an effect on catalysis property. The removal efficiency of Cu/A is much lower than Cu/PMO and Cu/A@Et-PMO/H$_2$O$_2$ due to the micropore channels and low porosity. Although the removal efficiency of Cu/PMO/H$_2$O$_2$ was more than 85%, its removal rate was lower than Cu/A@Et-PMO/H$_2$O$_2$. It is mainly attributed to the internal core zeolite A of Cu/A@Et-PMO which can provide more hydroxyl groups and can disperse a certain amount of metal nanoparticles [38]. Hence, these comparative results indicate that Cu/A@Et-PMO can serve as a suitable and powerful catalyst candidate for dye removal purposes.

The efficient degradation of substrate MB was ascribed to the decomposition H$_2$O$_2$ activated to generate hydroxyl radical with Cu$^0$ and Cu$^+$ and the synergy from adsorption properties of catalysts. The reaction mechanism was described as equation (3) (4) (5) [39]. To begin with, the dye MB molecules were adsorbed on the Et-PMO shell even the surface of interal core zeolite A by the pore channels and electrostatic interactions. Then the Feton-like active sites of Cu$^0$ can produce Cu$^+$ catalyze H$_2$O$_2$ decomposition to generate ·OH radicals, contributing to degradation and mineralization of MB by intramolecule electron transfer as follows the equation (6) [10]. At the same time, the free electron tranfering between active centers can promote the Fenton-like catalytic

performance. In addition, the porous frameworks of Cu/A@Et-PMO expose abundant active sites and can provide void space to facilitate the electron transfer via nanoparticles, further improving the catalytic property.

$$Surface \quad Cu^0 + H_2O_2 \rightarrow Cu^{2+} + 2OH \tag{3}$$

$$Cu^{2+} + H_2O_2 \rightarrow Cu^+ + H^+ + HO_2^\bullet \tag{4}$$

$$Cu^+ + H_2O_2 \rightarrow Cu^{2+} + OH + HO^\bullet \tag{5}$$

$$^\bullet OH + MB \rightarrow CO_2 + H_2O + degradation\ production \tag{6}$$



**Figure 6**. (**a**) The removal of 100 mg/L MB: H, A, P, SiO₂ refer to H₂O₂, Cu/A, Et-PMO, Cu/SiO₂, respectively. Reaction conditions: 30 mL of 60 mg/L MB, 3 mL of H₂O₂, 30 mg catalysts at room temperature 25℃; (**b**) the reusability of Cu/A@Et-PMO in the degradation of MB. Reaction conditions: 10 mL of 60 mg/L MB, 1 mL of H₂O₂, 10mg catalysts at room temperature 25℃. Error bars were made from three repeat trials.

*3.5 The recyclability of A@Cu@Et-PMO*

The recyclability of catalysts is an important factor in evaluating their practical applications. The reusability experiment of Cu/A@Et-PMO was carried out. In the first run, a high degradation rate for Cu/A@Et-PMO Cu/A up to 98.3%. The third and forth removal efficiency were 72.3% and 68.4%, as show in Figure 6b. The reason of decreasing degradation rate may be attributed to the one is, the reduction of adsorption and catalytic active sites in result of deposits from the degradation residuce on the surface of Cu/A@Et-PMO [40, 41]. The another is that the accumulation of acid intermediates significantly enhances the Cu leaching during the reacting process and leads to the decreasing of metal species in the Fenton like reaction under the heterogeneous reaction [42]. Besides, it can also be owe to the loss of catalysts in each cycle. More importantly, Figure 6b shows that the removal efficiency of MB on Cu/A@Et-PMO was still over 65% after four consecutive cycles. All of the above results further indicate that Cu/A@Et-PMO has a good reusability for the removal organic dye contaminant from effluent.

**4. Conclusions**

In summary, we have prepared a novel yolk-shell structure micro/mesopore composite combined with a core of the pristine zeolite A and an outer shell based on periodic mesoporous organosilica with ethyl groups (Et-PMO) via two step routes involving a modified StÖber method and an organosilane-directed growth-induced etching strategy. Subsequently, the Cu and $Cu_2O$ was loaded by means of the impregnation and reduction. The fabricated nanomaterial which can provide massive micro and mesopores has high special surface area and big pore volume and can be used to remove the organic dye MB in a heterogeneous Fenton-like reaction with $H_2O_2$. Compared to Cu/A and Cu/SiO$_2$, it shows high adsorption capacity and degradation efficiency. Moreover, the Cu/A@Et-PMO exhibits better recyclability reusing for four cycle experiments. Overall, the study can provide a model for heterogeneous catalytic reaction in moderate environment and could helps drive the development of the Fenton-like reaction.

References

1.    Wang, J. H.; Shao, X. Z.; Tian, G. H.; Bao, W. R. Preparation, characterization and excellent catalytic activity of Cu/SBA-15 nanomaterials. *Journal of Porous Materials*. **2018**, *25*, 207-214.

2.    Shimizu, K.; Sawabe, K.; Satsuma, A. Unique catalytic features of Ag nanoclusters for selective NOx reduction and green chemical reactions. *Catalysis Science & Technology*. **2011**, *1*, 331-341.

3.    Chi, Y.; Zhao, L.; Yuan, Q.; Li, Y. J.; Zhang, J. N.; Tu, J. C.; Li, N.; Li, X. T. Facile encapsulation of monodispersed silver nanoparticles in mesoporous compounds. *Chemical engineering journal*. **2012**, *195*, 254-260.

4.    Saad, R.; Thiboutot, S.; Ampleman, G.; Dashan, W.; Hawari, J. Degradation of trinitroglycerin (TNG) using zero-valent iron nanoparticles/nanosilica SBA-15 composite (ZVINs/SBA-15). *Chemosphere*. **2010**, *81*, 853-858.

5.    Ma, J.; Yu, F.; Zhou, L.; Yang, M. X.; Luan, J. S.;Tang, Y. H.; Fan, H. B.; Yuan, Z. W.; Chen, J. H. Enhanced adsorptive removal of methyl orange and methylene blue from aqueous solution by alkali-activated multiwalled carbon nanotubes. *ACS applied materials & interfaces*. **2012**, *4*, 5749-5760.

6.    Chen, T.; Xiong, Y. H.; Qin, Y. M.; Yang, H. G.;Zhang, P.; Ye F. G. Facile synthesis of low-cost biomass-based $\gamma$-Fe $_2O_3$/C for efficient adsorption and catalytic degradation of methylene blue in aqueous solution. *RSC Advances*. **2017**, *7*, 336-343.

7.    Neamtu, M.; Catrinescu, C.; Kettrup, A. Effect of dealumination of iron (III)—exchanged Y zeolites on oxidation of Reactive Yellow 84 azo dye in the presence of hydrogen peroxide. *Applied Catalysis B: Environmental*. **2004**, *51*, 149-157.

8.    Perez, M.; Torrades, F.; Domenech, X.; Domenech, X.; Peral, J. Fenton and photo-Fenton oxidation of textile effluents. *Water research*. **200**2, *36*, 2703-2710.

9.    Salem, I. A. Kinetics of the oxidative color removal and degradation of bromophenol blue with hydrogen peroxide catalyzed by copper (II)-supported alumina and zirconia. *Applied Catalysis B: Environmental*. **2000**, *28*, 153-162.

10.   Zhou, L. C.; Shao, Y. M.; Liu, J. R.; Ye, Z. F.; Zhang H.; Ma, J. J.; Jia, Y.; Gao, W, G.; Li, Y. F. Preparation and characterization of magnetic porous carbon microspheres for removal of methylene blue by a heterogeneous Fenton reaction. *ACS applied materials & interfaces*. **2014**, *6*, 7275-7285.

11.   Oliveira, R. L.; Shakeri, M.; Meeldijk, J. D.; de Jong, K. P.; de Jongh, P. E. Mapping nanocavities in plugged SBA-15 with confined silver nanostructures. *Microporous and Mesoporous Materials*. **2015**, *201*, 234-239.

12.   Lin, S.; Shi, L.; Yu, T. T.; Li, X. B.; Yi, X. F.; Zheng, A. M. Plug precursor assisted synthesis: A highly efficient method of tuning the acidic and structural properties of Al-SBA-15. *Microporous and Mesoporous Materials*. **2015**, *207*, 111-119.

13.   Zhu, J. J.; Xie, X.; Carabineiro, S. A. C.; Tavares, P. B.; Figueiredo, J. L.; Schomacker, R.; Thomas, A. Facile one-pot synthesis of Pt nanoparticles/SBA-15: an active and stable material for catalytic applications. *Energy & Environmental Science*. **2011**, *4*, 2020-2024.

14.   Egeblad, K.; Christensen, C. H.; Kustova, M.; Christensen, C. H. Templating mesoporous zeolites. *Chemistry of Materials*. **2007**, *20*, 946-960.

15.   Pérez-Ramírez, J.; Christensen, C. H.; Egeblad, K.; Christensen, C. H.; Groen, J. C. Hierarchical zeolites: enhanced utilisation of microporous crystals in catalysis by advances in materials design. *Chemical Society Reviews*. **2008**, *37*, 2530-2542.

16.   Tao, Y. S.; Kanoh, H. F.; Abrams, L.; Kaneko, K. Mesopore-modified zeolites: preparation, characterization, and applications. *Chemical reviews*. **2006**, *106*, 896-910.

17.   Hao, N.; Wang, H. T.; Webley, P. A.; Zhao, D. Y. Synthesis of uniform periodic mesoporous organosilica hollow spheres with large-pore size and efficient encapsulation capacity for toluene and the large biomolecule bovine serum albumin. *Microporous and Mesoporous Materials*. **2010**, *132*, 543-551.

18.   Dahaghin, Z.; Mousavi, H. Z.; Sajjadi, M. Synthesis and application of a novel magnetic SBA-15 nanosorbent for heavy metal removal from aqueous solutions. *Journal of Sol-Gel Science and Technology*. **2018**, *86*, 217-225.

19.   Ghosh, B. K.; Hazra, S.; Naik, B.; Ghosh, N. N. Preparation of Cu nanoparticle loaded SBA-15 and their excellent catalytic activity in reduction of variety of dyes. *Powder Technology*. **2015**, *269*, 371-378.

20.   Hajiaghababaei, L.; Badiei, A.; Ganjali, M. R.; Heydari, S.; Khaniani, Y.; Ziarani, G. M. Highly efficient removal and preconcentration of lead and cadmium cations from water and wastewater samples using ethylenediamine functionalized SBA-15. *Desalination*. **2011**, *266*, 182-187.

21.   Shin, J. H.; Park, S. S.; Selvaraj, M.; Ha, C. S. Adsorption of amino acids on periodic mesoporous organosilicas. *Journal of Porous Materials*. **2012**, *19*, 29-35.

22.   Rana, V. K.; Selvaraj, M.; Parambadath, S.; Chu, S. W.; Park, S. S.; Mishra, S.; Singh, R. P.; Ha, C. S. Heterocyclic tri-urea isocyanurate bridged groups modified periodic mesoporous organosilica synthesized for Fe (III) adsorption. *Journal of Solid State Chemistry*. **2012,** *194*, 392-399.

23.  Zou, H. B.; Sun, Q. L.; Fan, D. Y.; Fu. W. W.; Liu, L. J.; Wang, R. W. Facile synthesis of Yolk/Core-Shell structured TS-1@ Mesosilica composites for enhanced hydroxylation of phenol. **Catalysts**. **2015**, *5*, 2134-2146.

24.  Wei, Y.; Li, X. M.; Elzatahry, A. A.; Zhang, R. Y.; Wang, W. X.; Tang, X. T.; Yang, J. P.; Wang, J. X.; Al-Dahyan, D.; Zhao, D.Y. A versatile in situ etching-growth strategy for synthesis of yolk–shell structured periodic mesoporous organosilica nanocomposites. *RSC Advances*. **2016**, *6*, 51470-51479.

25.  Teng, Z. G.; Su, X. D.; Zheng, Y. Y.; Zhang, J. J.; Liu, Y.; Wang, S. J.; Wu, J.; Chen, G. T.; Wang, J. D.; Zhao, D. Y.; Lu, G. M. A facile multi-interface transformation approach to monodisperse multiple-shelled periodic mesoporous organosilica hollow spheres. *Journal of the American Chemical Society*. **2015**, *137*, 7935-7944.

26.  Dai, J. Y.; Zou, H. B.; Wang, R. W.; Wang, Y.; Shi, Z. Q.; Qiu, S. L. Yolk–shell $Fe_3O_4@SiO_2@PMO$: amphiphilic magnetic nanocomposites as an adsorbent and a catalyst with high efficiency and recyclability. *Green Chemistry*. **2017**, *19*, 1336-1344.

27.  Yu, H. J.; Lv, Y. Y.; Ma, K. Y.; Wang, C. G.; Xue, Z. T.; Zhao, Y. J.; Deng, Y. H.; Dai, Y.; Zhao, D. Y. Synthesis of core–shell structured zeolite-A@ mesoporous silica composites for butyraldehyde adsorption. *Journal of colloid and interface science.* **2014**, *428*, 251-256.

28.  Lopes, J. H.; Nogueira, F. G. E.; Gonçalves, M.; Oliveira, L. C. Modified Zeolite with Transition Metals Cu and Fe for Removal of Methylene Blue from Aqueous Medium: Mass Spectrometry Study. *Bulletin of Chemical Reaction Engineering & Catalysis*, **2015**, *10*, 237-248.

29.  Zou, H. B.; Wang, R. W.; Li, X. X.; Wang, X.; Zeng, S. J.; Li, L.; Zhang, Z. T.; Qiu, S. L. An organosilane-directed growth-induced etching strategy for preparing hollow/yolk–shell mesoporous organosilica nanospheres with perpendicular mesochannels and amphiphilic frameworks. *Journal of Materials Chemistry A*. **2014**, *2*, 12403-12412.

30.  Gan, T.; Wang, Z. K.; Shi, Z. X.; Zheng, D. Y.; Sun, J. Y.; Liu, Y. M. Graphene oxide reinforced core–shell structured Ag@ $Cu_2O$ with tunable hierarchical morphologies and their morphology–dependent electrocatalytic properties for bio-sensing applications. *Biosensors and Bioelectronics*. **2018**, *112*, 23-30.

31.  Do, Q. C.; Kim, D. G.; Ko, S. O. Nonsacrificial Template Synthesis of Magnetic-Based Yolk–Shell Nanostructures for the Removal of Acetaminophen in Fenton-like Systems. *ACS applied materials & interfaces*. **2017**, *9*, 28508-28518.

32.  Wang, J.; Liu, C.; Tong, L.; Li, J. S.; Luo, R.; Qi, J. W.; Li, Y.; Wang, L. J. Iron–copper bimetallic nanoparticles supported on hollow mesoporous silica spheres: an effective heterogeneous Fenton catalyst for orange II degradation. *RSC Advances*. **2015**, *5*, 69593-69605.

33.  Dong, C. S.; Zhong, M. L.; Huang, T.; Ma, M. X.; Wortmann, D.; Brajdic, M.; Kelbassa, I. Photodegradation of methyl orange under visible light by micro-nano hierarchical $Cu_2O$ structure fabricated by hybrid laser processing and chemical dealloying. *ACS applied materials & interfaces.* **2011**, *3*, 4332-4338.

34.  Tang, X. K.; Feng, Q. M.; Liu, K.; Li, Z. S.; Wang, H. Fabrication of magnetic $Fe_3O_4$/silica nanofiber composites with enhanced Fenton-like catalytic performance for Rhodamine B degradation. *Journal of Materials Science.* **2018**, *53*, 369-384.

35.  Vinothkannan, M.; Karthikeyan, C.; Gnana kumar, G.; Kim, A. R.; Yoo, J. D. One-pot green synthesis of reduced graphene oxide (RGO)/$Fe_3O_4$ nanocomposites and its catalytic activity toward methylene blue dye degradation. *Spectrochimica Acta Part A: Molecular and Biomolecular Spectroscop*y. **2015**, *136*, 256-264.

36.  Nassar, M. Y.; Abdelrahman, E. A. Hydrothermal tuning of the morphology and crystallite size of zeolite nanostructures for simultaneous adsorption and photocatalytic degradation of methylene blue dye. *Journal of Molecular Liquids.* **2017**, *242*, 364-374.

37.  Wang, J.; Liu, C.; Hussain, I.; Li, C.; Li, J. S.; Sun, X. Y.; Shen, J. Y.; Han,W. Q.; Wang, L. J. Iron–copper bimetallic nanoparticles supported on hollow mesoporous silica spheres: the effect of Fe/Cu ratio on heterogeneous Fenton degradation of a dye. *RSC Advances*, **2016**, *6*, 54623-54635.

38.  Nassar, M. Y.; Ahmed, I. S.; Samir, I. A novel synthetic route for magnesium aluminate (MgAl$_2$O$_4$) nanoparticles using sol–gel auto combustion method and their photocatalytic properties. *Spectrochimica Acta Part A: Molecular and Biomolecular Spectroscopy.* **2014**, *131*, 329-334.

39.  Wang, S.; Liu, L. Fabrication of novel nanoporous copper powder catalyst by dealloying of ZrCuNiAl amorphous powders for the application of wastewater treatments. *Journal of hazardous materials,* **2017**, *340*, 445-453.

40.  Deng, J. H.; Wen, X. H.; Wang, Q. Solvothermal in situ synthesis of Fe$_3$O$_4$-multi-walled carbon nanotubes with enhanced heterogeneous Fenton-like activity. *Materials Research Bulletin.* **2012**, *47*, 3369-3376.

41.  Jafari, A. J.; Kakavandi, B.; Jaafarzadeh, N.; Kalantary, R. R.; Ahmadi, M.; Babaei, A. A. Fenton-like catalytic oxidation of tetracycline by AC@Fe$_3$O$_4$ as a heterogeneous persulfate activator: adsorption and degradation studies. *Journal of Industrial and Engineering Chemistry.* **2017**, *45*, 323-333.

42.  Zhan, Y. Z.; Zhou, X.; Fu, B.; Chen, Y. L. Catalytic wet peroxide oxidation of azo dye (Direct Blue 15) using solvothermally synthesized copper hydroxide nitrate as catalyst. *Journal of hazardous materials.* **2011**, *187*, 348-354.